Macromolecules

Article

pubs.acs.org/Macromolecules

N-Type Hyperbranched Polymers for Supercapacitor Cathodes with Variable Porosity and Excellent Electrochemical Stability

David F. Zeigler,[†] Stephanie L. Candelaria,[‡] Katherine A. Mazzio,[‡] Trevor R. Martin,[‡] Evan Uchaker,[‡] Sabin-Lucian Suraru,[‡] Lauren J. Kang,[†] Guozhong Cao,[‡] and Christine K. Luscombe*[,†,‡]

[†]Department of Chemistry and [‡]Department of Materials Science and Engineering, University of Washington, Seattle, Washington 98195, United States

Supporting Information

ABSTRACT: A series of n-type hyperbranched polymers exhibiting variable porosity and excellent electrochemical stability are presented for use as the cathodes of asymmetric supercapacitors. The polymers are designed with triphenylamine (TPA) cores and naphthalene diimide (NDI) terminal units, with NDI being chosen for its electrochemical stability under reduction. A different number of thiophene rings between the TPA and NDI units are used to alter the porosity. These devices show very good stability over 500 cycles as a result of the stable NDI unit, and nitrogen adsorption experiments confirm that the addition of thiophene spacers results in a concomitant increase in the polymer matrix pore size. Electrochemical impedance spectroscopy (EIS) characterization reveals that as the porosity of the polymer increases, the diffusion resistance decreases. However, as the pore size increases, the charge transfer resistance and equivalent series resistance increases. Finally, one of the polymers is used to fabricate proof-of-concept symmetric supercapacitors.

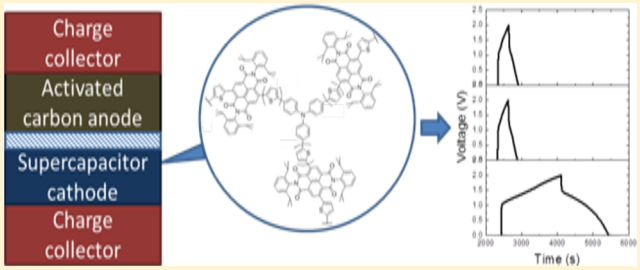

1. INTRODUCTION

As the global human population and our reliance upon electronic devices increase, energy demands continue to grow.[1−3] Concurrently, it has become clear that fossil fuels, our current major sources of energy, are unsustainable both financially and environmentally.[4] As a result, there has been growing interest in renewable energy resources. Some of the most promising renewable energy candidates, such as solar and wind power, provide energy intermittently over the course of the day, requiring the parallel development of efficient energy storage technologies. The most common storage devices are batteries, such as lead-acid and lithium-ion batteries.[5−9] These devices can have inherent problems, however, including being time-consuming to charge and unable to deliver energy at high rates, as well as exhibiting reduction in discharge capacity over time. Typical batteries can withstand 500−1000 cycles before they lose 20% of their energy density.[10] These factors limit their adoption in certain applications. As a result, there is a growing need for innovative energy storage devices that can rapidly deliver energy when needed, while simultaneously being inexpensive to manufacture, produced from sustainable materials, and stable to repeated galvanic cycling.

Supercapacitors are an attractive alternative to batteries because they possess high power densities, rapid charge/discharge rates, and good stability, with device lifetimes typically on the order of 10^5 cycles.[11−15] Presently, the benchmark electrode material for supercapacitors is activated carbon. Activated carbon is extremely stable under a variety of conditions, has reasonably high conductivities, and is inherently highly porous. However, the performance of activated carbon suffers because it can only store charge through double-layer capacitance, and many of its pores can be inaccessible or too small to accommodate solvated electrolyte ions; these two characteristics limit the energy densities of activated carbon-based supercapacitors.[16−18] Other forms of conductive carbon (e.g., aerogels, nanotubes, graphene) have been explored but typically attain specific capacitances comparable to those of activated carbon.[19−24]

To meet the requirements of many applications, the energy densities of supercapacitors need to be increased. One method to boost the specific capacitance and energy density of a supercapacitor is to utilize pseudocapacitance, where energy is stored via surface redox processes between the electrode and the ions in the electrolyte.[13,14] Pseudocapacitance can boost the energy density of supercapacitors significantly. Two main materials that have been utilized in supercapacitors to take advantage of pseudocapacitance are metal oxides and conductive polymers. While metal oxides can achieve impressively high specific capacitances, they often suffer from high cost and limited abundance of materials.[12,25−31] Conductive polymers offer an attractive alternative to metal oxides because they can be synthesized from plentiful materials at low cost.[32] A variety of conductive polymers have been investigated as supercapacitor electrodes in type I, II, III, and IV

Received: May 19, 2015
Revised: July 15, 2015
Published: July 27, 2015

DOI: 10.1021/acs.macromol.5b01070
Macromolecules 2015, 48, 5196−5203

architectures, including polythiophene,[33−37] polyaniline,[38] and polypyrrole[39,40] derivatives as well as alternating donor−acceptor polymers.[41,42] Most conductive polymers have limited utility for supercapacitor applications because they are typically p-type and degrade upon reduction, prohibiting their use as the negative electrode of the supercapacitor.[13,14] As a result, asymmetric type IV architectures exploiting n-type materials or modified p-type polymers that are more amenable to reduction have been explored.[43−45] The polymers used for supercapacitor applications have almost exclusively been linear polymers that exhibit good $\pi-\pi$ stacking, which inevitably minimizes the amount of interstitial space within the polymer matrix. While good $\pi-\pi$ stacking results in polymers with high conductivities, it also hinders electrolyte diffusion, which thereby limits charge stored through double-layer capacitance and the site-specific kinetics of the pseudocapacitive charging process. Thus, polymer-based supercapacitors generally have limited charge storage capacities compared to activated carbon supercapacitors.[12]

Considering these limitations, it is desirable to generate n-type or ambipolar conductive and electrochemically stable polymers with controllable pore sizes for optimization of the surface area and diffusion rates of solvent and electrolyte molecules. Herein we report the synthesis of a series of three n-type triphenylamine (TPA)/napthalene diimide (NDI) based hyperbranched polymers with a differing number of thiophene spacers between the TPA and NDI monomers through solution-based Stille polymerizations. The polymers were characterized by cyclic voltammery and used to fabricate both symmetric and asymmetric supercapacitors. The electrochemical properties, galvanostatic cycling behavior, and stability of the devices were determined. The devices were further analyzed using electrochemical impedance spectroscopy (EIS).

2. EXPERIMENTAL SECTION

Materials and Characterization. Unless otherwise specified, all chemicals were purchased from Aldrich or TCI and used without further purification. *N,N*-Di-(2,6-diisopropylphenyl)-2,6-dibromonaphthalene-1,4,5,8-tetracarboxylic acid bisimide,[46] tris(4-bromophenyl)amine, tris[4-(4,4,5,5-tetramethyl-1,3,2-dioxaborolan-2-yl)phenylamine,[47] tris(4-tributylstannylphenyl)amine,[48] tris(4-(thiophen-2-yl)phenyl)amine, and tris(4-(2,2′-bithiophen-2-yl)phenyl)-amine[49] were prepared according to the literature. ^{1}H NMR spectra were collected on a Bruker AV 300 spectrometer operating at 300 MHz in deuterated chloroform solution with TMS as reference. Polymer molecular weights were measured by a gel permeation chromatograph (GPC) with a refractive index detector at room temperature and THF as the eluent using the conventional calibration technique with five narrow polystyrene standards. Cyclic voltammograms of polymer films were conducted on a BAS CV-50W voltammetric system with a three-electrode cell in acetonitrile with 0.1 M tetrabutylammonium hexafluorophosphate (Bu_4NPF_6) and using a scan rate of 10 mV s^{-1}. ITO, Ag/$AgNO_3$, and Pt wire were used as working, reference, and counter electrodes, respectively. Nitrogen sorption was analyzed using a Quantachrome NOVA 4200e surface area analyzer. All spectra were plotted using OriginPro 8. EIS was performed on the symmetric and asymmetric supercapacitor devices (see fabrication protocol below). EIS was measured with an ac voltage amplitude of 10 mV and frequency range of 0.1 MHz−1 mHz. The sample was pretreated at 2 V for 10 min prior to the scan. Cyclic stability tests were performed after completing the CVs, GCs, and EIS measurements. Samples were subjected to repeated charge and discharge during galvanic cycling at 0.1 mA up to 500 cycles.

Synthesis of *N,N*-Di-(2,6-diisopropylphenyl)-2,6-dithienylnaphthalene-1,4,5,8-tetracarboxylic Acid Bisimide. *N,N*-Di-(2,6-diisopropylphenyl)-2,6-dibromonaphthalene-1,4,5,8-tetracarboxylic acid bisimide (6 mmol), 2-tributylstannylthiophene (18 mmol), and toluene (20 mL) were added to a flask. The contents were evacuated and backfilled with N_2 three times before quickly adding $Pd(PPh_3)_4$ (0.6 mmol). The mixture was heated to 100 °C and stirred for 24 h. After cooling, the mixture was filtered through a silica plug, concentrated, and purified by silica gel chromatography ($CHCl_3$:Hex 3:1) to yield a bright red solid. Yield: 76%. ^{1}H NMR (300 MHz, methylene chloride-d_2) δ: 8.83 (s, 2H), 7.55−7.46 (m, 4H), 7.37 (m, 6H), 7.12 (dd, J = 5.1, 3.6 Hz, 2H), 2.73 (hept, J = 6.9 Hz, 4H), 1.12 (d, J = 6.8 Hz, 24H).

Synthesis of *N,N*-Di-(2,6-diisopropylphenyl)-2,6-(2-bromothienyl)-naphthalene-1,4,5,8-tetracarboxylic Acid Bisimide. *N,N*-Di-(2,6-diisopropylphenyl)-2,6-dithienylnaphthalene-1,4,5,8-tetracarboxylic acid bisimide (2 mmol) was dissolved in chloroform and cooled on an ice bath in the dark to protect from ambient sunlight. NBS (4.4 mmol) was dissolved in chloroform and then added dropwise. The mixture was allowed to warm to room temperature and stirred for 16 h. The solution was poured into water, extracted, and the combined organic extracts were dried with Na_2SO_4 and concentrated. The residue was purified by column chromatography (($CHCl_3$:Hex 3:2) to yield a bright red solid. Yield: 83%. ^{1}H NMR (300 MHz, methylene chloride-d_2) δ: 8.81 (s, 2H), 7.48 (dd, J = 8.3, 7.2 Hz, 2H), 7.33 (s, 2H), 7.31 (s, 2H), 7.16−7.01 (m, 4H), 2.70 (hept, J = 6.8 Hz, 4H), 1.12 (d, J = 6.8 Hz, 24H).

Synthesis of TPA-1Th-NDI Polymer. *N,N*-Di-(2,6-diisopropylphenyl)-2,6-(2-bromothienyl)naphthalene-1,4,5,8-tetracarboxylic acid bisimide (1.2 mmol), tris(3-tributylstannyl)phenylamine (0.30 mmol), and toluene (10 mL) were added to a flask. The contents were evacuated and backfilled with N_2 three times before quickly adding $Pd(PPh_3)_4$ (0.03 mmol). The mixture was heated to 120 °C and stirred for 72 h. After cooling, the mixture was poured into methanol and filtered. The solid was collected and Soxhlet extracted with methanol (24 h), acetone (24 h), and hexanes (24 h). The remaining solid was collected, yielding a dark solid. Yield: 37%. GPC: M_w = 4300, M_n = 300. ^{1}H NMR (300 MHz, chloroform-d) δ: 8.98−8.83 (bm), 7.53−7.25 (bm), 7.09 (bm), 2.90−2.62 (bm), 1.31−1.05 (bm).

Synthesis of TPA-2Th-NDI Polymer. Tris(4-(thiophen-2-yl)-phenyl)amine (0.3 mmol) was dissolved in THF (30 mL) and cooled to −78 °C before adding *n*-BuLi (0.93 mmol, 3.1 equiv) dropwise. The solution was stirred at −78 °C for 2 h. In one portion, tributyltin chloride (0.95 mmol, 3.2 equiv) was then added, and the solution was allowed to warm to room temperature and stirred overnight. The solution was then poured into water and extracted with ether. The combined organic solvents were dried over Na_2SO_4, concentrated, and used without further purification. This material was added to *N,N*-di-(2,6-diisopropylphenyl)-2,6-(2-bromothienyl)naphthalene-1,4,5,8-tetracarboxylic acid bisimide (1.2 mmol) and toluene (10 mL) in a three-neck flask. The contents were evacuated and backfilled with N_2 three times before quickly adding $Pd(PPh_3)_4$ (0.03 mmol). The mixture was heated to 120 °C and stirred for 72 h. After cooling, the mixture was poured into methanol and filtered. The solid was Soxhlet extracted with methanol (24 h), acetone (24 h), and hexanes (24 h). The remaining solid was collected, yielding a dark solid. Yield: 32%. GPC: M_w = 7300, M_n = 500. ^{1}H NMR (300 MHz, chloroform-d) δ: 8.96−8.80 (bm), 7.48 (bm), 7.38−7.28 (bm), 7.15 (bm), 2.76 (bm), 1.33−0.99 (bm).

Synthesis of TPA-3Th-NDI Polymer. Tris(4-(2,2′-bithiophen-2-yl)phenyl)amine (0.4 mmol) was dissolved in THF (40 mL) and cooled to −78 °C before adding *n*-BuLi (1.24 mmol, 3.1 equiv) dropwise. The solution was stirred at −78 °C for 2 h before quickly adding tributyltin chloride (1.27 mmol, 3.2 equiv) in one portion. This solution was then allowed to warm to room temperature and was stirred overnight before pouring into water and extracting with ether. The combined organic solvents were dried over Na_2SO_4, concentrated, and used without further purification. This material was added to *N,N*-di-(2,6-diisopropylphenyl)-2,6-(2-bromothienyl)naphthalene-1,4,5,8-tetracarboxylic acid bisimide (1.6 mmol) and toluene (15 mL) in a three-neck flask. The contents were evacuated and backfilled with N_2 three times before rapidly adding $Pd(PPh_3)_4$ (0.03 mmol). The

DOI: 10.1021/acs.macromol.5b01070
Macromolecules 2015, 48, 5196−5203

Scheme 1. Synthesis of TPA-(*n*)Th-NDI Polymers[a]

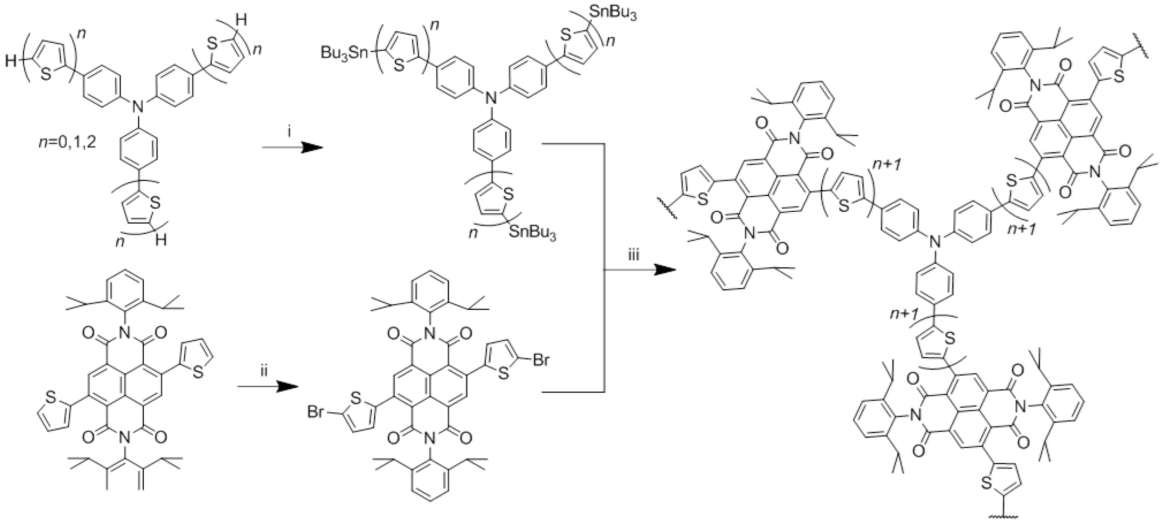

[a]Reagents and conditions: (i) (1) *n*-BuLi, THF, 1 h, −78 °C, (2) $ClSnBu_3$, rt, overnight; (ii) NBS, $CHCl_3$, 24 h, 87%; (iii) $Pd(PPh_3)_4$, toluene, 120 °C, 3 days, 32−45%.

mixture was heated to 120 °C and stirred for 72 h. After cooling, the mixture was poured into methanol and filtered. The solid was Soxhlet extracted with methanol (24 h), acetone (24 h), and hexanes (24 h). The remaining solid was collected, yielding a dark solid. Yield: 45%. GPC: M_w = 5700, M_n = 500. ^{1}H NMR (300 MHz, chloroform-*d*) δ: 8.90 (bm), 7.58−7.30 (bm), 7.22−7.03 (bm), 2.85−2.67 (bm), 1.37−1.08 (bm).

Activated Carbon Synthesis. Activated carbon was prepared through sol−gel processing from precursors resorcinol and furaldehyde using hexamethylenetetramine (HTMA) as the catalyst. The procedure for synthesizing this activated carbon is similar to that reported elsewhere.[50,51] The furaldehyde to resorcinol molar ratio is set to 2.5, and the resorcinol to hexamine molar ratio is 50. The resorcinol and furaldehyde are mixed together first, followed by the addition of the solvent *tert*-butanol. HTMA is added last as the reactive catalyst. The mixture is sealed and cured in an oven at 80 °C for 7 days to allow for gelation. The gel was then freeze-dried under vacuum at −50 °C in a Labconco FreeZone 1 L freeze-dryer. Pyrolysis was performed under N_2 with a ramp rate of 5 °C/min to a maximum temperature of 900 °C for 180 min. Activation occurred under dry air flow at 420 °C for 240 min with a ramp rate of 5 °C/min, followed by heating again at 900 °C for 180 min under N_2 flow to remove any new functional groups that may have formed during activation.

Supercapacitor Fabrication. The polymer or activated carbon was ground with a mortar and pestle and mixed with 3 wt % polytetrafluoroethylene (PTFE) as a binder. The mixture was mechanically rolled into sheets with a thickness of 0.07−0.08 mm, and electrodes were punched out with a diameter of 10 mm. A Celgard 2400 porous film was used to separate the electrodes to prevent short circuiting and carbon-coated aluminum contacts were used as the current collectors. The two-electrode assembly was pressed under vacuum overnight to ensure good contact between the electrodes and the current collectors, in addition to removing any moisture from the porous electrodes. A 1 M tetraethylammonium tetrafluoroborate (TEATFB) in 1:1 propylene carbonate:dimethylcarbonate was used as the electrolyte. The electrode assembly was placed in a flat cell, and electrolyte was added in an argon-filled glovebox. The samples were then placed under vacuum to increase the penetration of the electrolyte into the pores.

3. RESULTS AND DISCUSSION

Increasing interest in supercapacitors has led to the exploration of novel electrode materials that can achieve higher specific capacitances than activated carbon materials. Conductive polymers are one such class of materials, which are highly attractive as supercapacitor electrodes due to the tunability of their electronic energy levels, charge transport properties, physical properties in the solid state, and their low cost. To the best of our knowledge, the first report of a hyperbranched polymer for a supercapacitor electrode was a report on the electropolymerization of a tris(thiophene)triphenylamine monomer to yield a porous polymer network for a supercapacitor anode.[52] The resulting electrodes possessed very high specific capacitances (near 1000 F/g), but the double-layer capacitance was found to only contribute ∼1−2 F/g. In addition, the polymers reported were p-type and therefore could only be used as the cathode in the device.

The structure of the conductive polymer discussed herein was chosen to satisfy several requirements: (1) variable porosity (to facilitate solvent/electrolyte diffusion, thereby optimizing redox kinetics and double-layer capacitance), (2) n-type/ambipolar, and (3) electrochemical stability. The latter two requirements brought our attention to NDIs which have proven good n-type and ambipolar properties in small molecule and polymeric semiconducting materials.[53,54] Moreover, well-established chemistry to introduce solubilizing groups at the imide position and convenient functionalization chemistry of the NDI core makes the NDI unit an ideal building block for our purpose.[55] It is noteworthy that TPA−NDI donor−acceptor small molecules have been shown to possess ambipolar charge transport and robust electrochemical stability.[56]

The geometry of the TPA unit introduces a hyperbranched structure to the polymer, which leads to ample interstitial space in the solid state. Additionally, it was hoped that adding thiophene spacers between the TPA and NDI moieties would enlarge the corresponding pores of the polymer matrix. Finally, the 2,6-diisopropylphenylimide groups were used to create a balance between solubility for the solution polymerization and congestion of the pores of the polymer matrix.

The synthesis (Scheme 1) began with the bromination of TPA, followed by lithiation and quenching with tributylstannyl chloride. This intermediate was coupled to 2-bromothiophene or 5-bromo-2,2′-bithiophene. The resultant compounds were

DOI: 10.1021/acs.macromol.5b01070
Macromolecules 2015, 48, 5196−5203

subsequently stannylated to yield three TPA-based monomers. Concurrently, naphthalene dianhydride was brominated and the anhydrides were converted to imides with 2,6-diisopropylaniline.[46,57] This molecule was coupled to thiophene at the bay positions using a Stille coupling and dibrominated with NBS.[58] The polymers were prepared by standard Stille polymerization conditions and named TPA-(n)Th-NDI, where (n) indicates the number of thiophene rings situated between the TPA and NDI units. GPC was used to determine relative molecular weights of the polymers, and all three polymers were found to have similar values (Experimental Section and Figure S5).

The electrochemical responses of the polymers were characterized via cyclic voltammetry using a standard three-electrode setup. Representative reduction scans can be found in Figure 1 and Figure S6 of the Supporting Information. Each

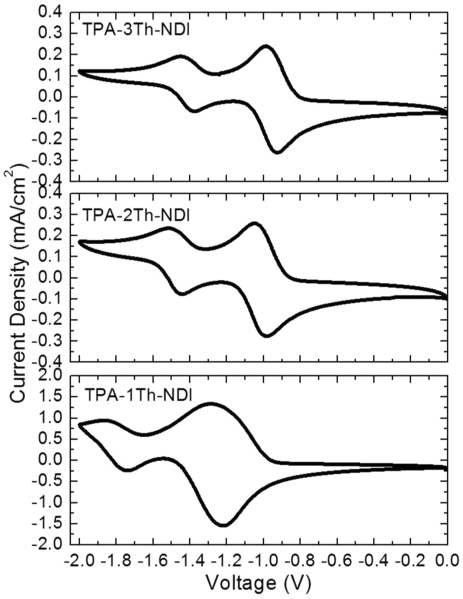

Figure 1. Cyclic voltammagrams of the three TPA-(n)Th-NDI polymer films taken at a scan rate of 10 mV s^{-1}.

polymer film was found to exhibit n-type behavior with two reversible reduction processes. The reduction potentials of TPA-1Th-NDI, TPA-2Th-NDI, and TPA-3Th-NDI taken at a scan rate of 10 mV s^{-1} are −1.4, −1.2, and −1.1 V, respectively, against the potential of the ferrocenium/ferrocene redox couple in acetonitrile (Figure S7). No clear oxidation waves were found within the available potential window (Figure S7). In addition, the current response of TPA-1Th-NDI is significantly larger than those of either TPA-2Th-NDI or TPA-3Th-NDI.

Because of the promising reductive responses of the polymers, they were first used to fabricate asymmetric supercapacitors with activated carbon at the positive electrode. The devices were subjected to galvanic cycling from 0 to 2 V, the first complete charge profile of which can be seen in Figure 2. The first full cycle features and exemplifies the differences between the different polymers, with the full range shown in Figure S8. The charge/discharge curves exhibit characteristics common to supercapacitors that store charge through pseudocapacitance, rather than only double-layer capacitance, as expected for these polymers. The capacitances of the devices were calculated according to eq 1:

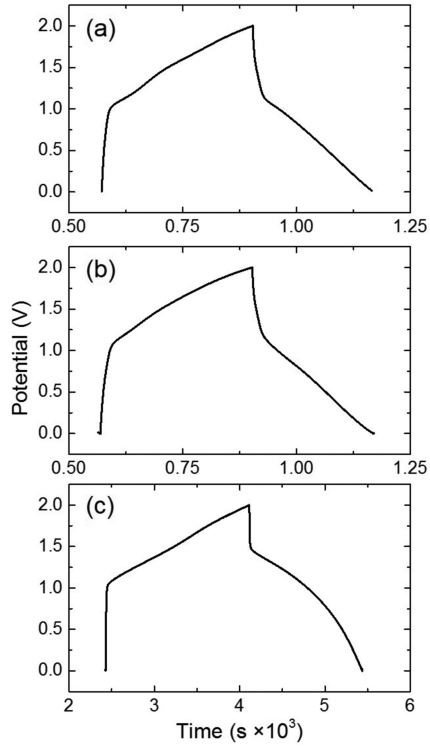

Figure 2. First complete galvanic cycling profile of the activated carbon-TPA-(n)Th-NDI asymmetric supercapacitor where (a) n = 3, (b) n = 2, and (c) n = 1.

$$C = \frac{4It}{Vm} \tag{1}$$

where C is the capacitance, I is the discharge current (constant at 0.1 mA), t is the discharge time, V is the change in voltage during discharge, and m is the mass of the polymer/binder electrode. The specific capacitance of the devices utilizing TPA-1Th-NDI, TPA-2Th-NDI, and TPA-3Th-NDI were found to be 22.0, 4.92, and 4.94 F/g, respectively. These values are significantly less than those for the more commonly reported polymer systems;[13,14] however, performance trends among the materials still remain of interest. Each asymmetrical device shows a quasi-triangular shape, which is characteristic of pseudocapacitive systems, where the capacitance derived from the reversible faradic reaction can be strongly potential dependent. The curvature in the voltage profile may arise because of distributed resistance through the porous electrode. All the TPA-(n)Th-NDI polymers suffer from activation polarization at the onset of current, which reflects the overpotential associated with an electrochemical process and is related to the activation energy associated with the electron transfer, partially contributing to the asymmetry of the charge−discharge profiles. TPA-1Th-NDI shows significantly longer charge and discharge times than the other two materials, leading to its much larger capacitance. There is also a noticeable increase in the voltage (IR) drop when the number of thiophene rings situated between the TPA and NDI units increases from one to two thiophenes, indicating that the more closely packed structure of TPA-1Th-NDI has improved electrical conductivity. It is also possible that less thiophene may provide more favorable chemistry to induce pseudocapacitive reactions in the material, thereby increasing capacitance. However, there is little change between TPA-2Th-NDI and

DOI: 10.1021/acs.macromol.5b01070
Macromolecules 2015, 48, 5196−5203

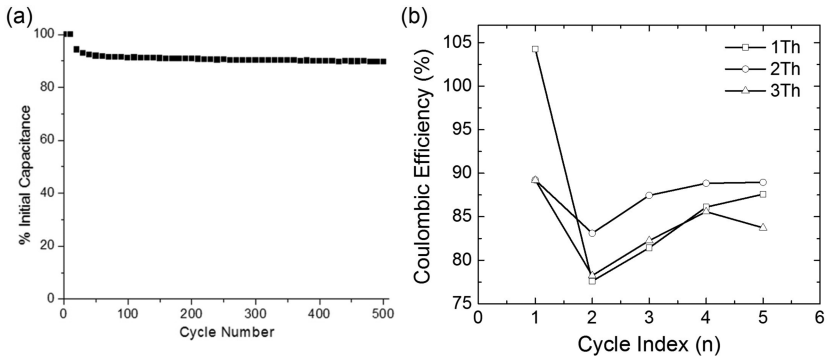

Figure 3. Stability of asymmetric supercapacitor (a) in terms of capacitance retention upon cycling for the TPA-1Th-NDI polymer and (b) Coulombic efficiency for all TPA-*n*Th-NDI polymers.

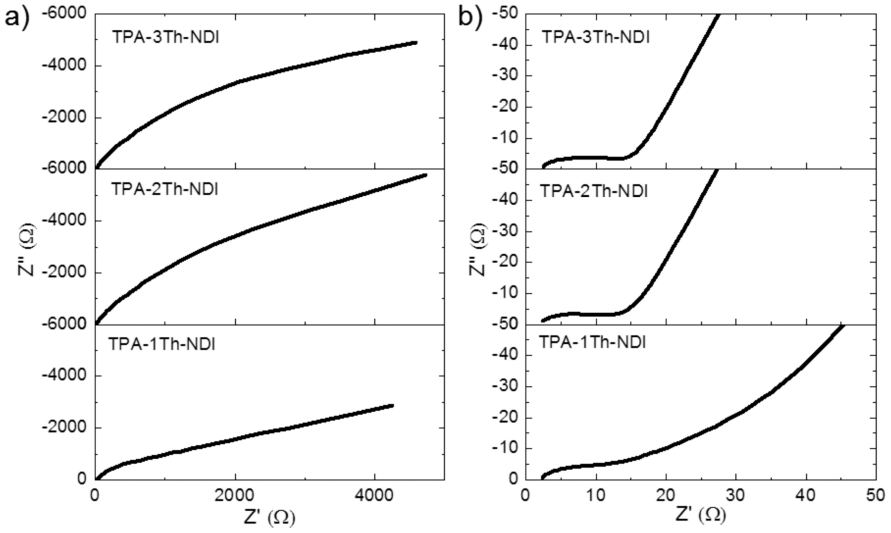

Figure 4. Nyquist plots of TPA-(*n*)Th-NDI polymers (a) over the entire frequency range and (b) at high frequencies.

TPA-3Th-NDI, suggesting that there is a point at which the incorporation of additional thiophene rings no longer has an effect on the electrochemical performance of the material.

Because the TPA-1Th-NDI device showed the highest specific capacitance, we investigated its stability to repeated cycling. As can be seen in Figure 3a, we found that our TPA-1Th-NDI asymmetric capacitors exhibit losses of <10% of their original capacitance over 500 cycles. This is as good as or better than existing battery technologies and represents one of the most promising aspects of this material system.[12] The rate dependence is shown in Figure S9. All samples show a drop in capacitance initially but then level off as the current rate increases. Interestingly, TPA-1Th-NDI exhibits the greatest decrease in rate performance, indicating that this sample has increased resistance to charging and discharging. This may be due in part to lower surface area and smaller average pore size, hindering electrolyte diffusion and limiting charge storage. The Coulombic efficiency, however, shows a slightly different trend. The TPA-1Th-NDI device starts with a Coulombic efficiency exceeding 100% which then drops to ∼78% in the second cycle and steadily improves in the subsequent cycles. This is typically indicative that there are some irreversible surface reactions taking place, such as interfacial passivation, that could potentially result in a slight degree of structural rearrangement.[59−63] Passivation or reconstruction of the electrode surface could justify the drop in Coulombic efficiency incurred during the second cycle and the gradual stabilization that successively takes place.[64,65] Additionally, a decrease in the anodic current density is consistent with passivation of the electrode.[66,67] The TPA-2Th-NDI and TPA-3Th-NDI devices exhibit similar trends in terms of Coulombic efficiency, but to a lesser degree, illustrating the effects the (*n*)Th units can have on the redox processes.

To develop our understanding of the differences observed in the specific capacitances for the polymers examined, the devices were characterized using EIS, which is an effective way to determine the component resistances within a supercapacitor.[68] The EIS characterization of the devices over the entire frequency range can be found in Figure 4a. In this case, the straight line at midfrequencies corresponds to the linear diffusion process, more commonly known as the Warburg impedance, and provides a comparative evaluation of the diffusion coefficient values. The behavior of each of the polymers at lower frequencies deviates significantly from the vertical line that would be seen for an ideal supercapacitor, indicating large diffusion resistances. Among the three polymers, TPA-1Th-NDI has the qualitatively highest diffusion resistance, while TPA-2Th-NDI and TPA-3Th-NDI exhibit fairly similar behavior with the diffusion resistance being slightly lower for TPA-3Th-NDI. This suggests that a higher amount of thiophene units results in more open porosity, allowing electrolyte ions access to easier diffusion pathways within the

DOI: 10.1021/acs.macromol.5b01070
Macromolecules 2015, 48, 5196−5203

material. This is promising from a synthetic standpoint, as TPA-2Th-NDI and TPA-3Th-NDI were designed to have larger pore sizes than the TPA-1Th-NDI polymer through the inclusion of additional thiophene spacer units. At higher frequencies, as can be seen in Figure 4b, the diameter of the semicircle directly corresponds to the charge-transfer resistance at the electrode−electrolyte interface, and reveals somewhat high charge transfer resistances (R_{ct}) and equivalent series resistances (ESR) in these supercapacitors. Fitting to an equivalent circuit, the values were found to be 4.7, 6.5, and 9.2 Ω for the R_{ct} and 1.9, 2.1, and 2.3 Ω for the ESR for TPA-1Th-NDI, TPA-2Th-NDI, and TPA-3Th-NDI, respectively. In both cases, these resistances increased from TPA-1Th-NDI to TPA-3Th-NDI. We hypothesize that this increase in resistance across the series may be due to increasing thiophene content in the electrode materials, resulting in a significant decrease in their electron mobilities, which can generally be thought of as being due to a dilution of the n-type NDI moieties. This idea has been corroborated in other NDI-based materials where adding increasing numbers of thiophene rings to the NDI bay positions decreased their corresponding electron mobilities.[69] Such a decrease in the n-type character of the materials could adversely affect the ability to extract electrons from these materials, thereby increasing the ESR. In addition, because reduction is a site-specific process, it is reasonable to assume that adding thiophene spacers effectively decreases the number of locations where reduction can favorably occur, which we would expect to result in the observed increase in the R_{ct}.

The polymers were further characterized using nitrogen adsorption experiments to determine their pore sizes and specific surface areas, the results of which can be found in Figure S10. Using the Barrett−Joyner−Halenda (BJH)[70] desorption model, the pore diameters of TPA-1Th-NDI, TPA-2Th-NDI, and TPA-3Th-NDI were found to be 3.18, 3.72, and 4.22 nm, respectively. These values corroborate the synthetically designed effect of the addition of thiophene spacers, where increasing spacer content should result in increasing pore size. Meanwhile, the Brunauer−Emmett−Teller (BET) surface areas were 6.1, 20.4, and 20.2 $m^2\ g^{-1}$ for TPA-1Th-NDI, TPA-2Th-NDI, and TPA-3Th-NDI, respectively. The increasing surface area across the series further shows the effect of the thiophene spacers.

Finally, the TPA-1Th-NDI polymer was used to fabricate proof-of-concept symmetric supercapacitors. The electronic transitions within the symmetric supercapacitor were examined via cyclic voltammetry, as can be seen in Figures S7a and S8. The symmetric supercapacitor shows two main transitions, which, when overlaid with the reduction scans of the polymer (Figure S11b), it becomes clear that the transitions and general shape of the CV curve are a conflation of the reduction and oxidation scans. Galvanic cycling analysis of this device can be found in Figure S13a and shows that these devices exhibit a low capacitance of ∼0.5 F/g. The device again showed exceptional stability, losing only ∼10% of its charge storage capacity over >500 cycles (Figure S13b).

The cause of this low capacitance was investigated using EIS. The EIS characterization of the device revealed a very high R_{ct} of 420.3 Ω and an ESR of 7.7 Ω (Figure S14), which are significantly larger than that of the asymmetric devices. The very high R_{ct} value is likely the result of slow oxidative kinetics of the polymer at the positive electrode. Since the specific capacitance of the symmetric supercapacitor is dictated by the capacitance of the positive and negative electrodes, it is probable that the majority of the charge-transfer resistance occurs at the positive electrode. Because of the poor capacitance but excellent stability, these materials can be used as a springboard for future polymer systems, where ambipolar hyperbranched polymers with better mobility characteristics could help reduce R_{ct} while maintaining control over porosity and improving stability over repeated galvanic cycling.

4. CONCLUSION

A series of three hyperbranched polymers possessing TPA and NDI units were designed for use as the electrodes of symmetric and asymmetric supercapacitors. The polymers differed by the number of thiophene rings between the TPA and NDI units. Each polymer exhibited reversible reduction processes. Subsequently, asymmetric supercapacitors were fabricated using the polymers. The devices showed excellent stability over 500 cycles and predictable charge/discharge ability, but they were limited to moderate capacitances (up to 22 F/g). EIS characterization revealed that the devices had relatively low initial R_{ct} values (ca. 4.7−9.2 Ω) and ESR values (ca. 1.9−2.3 Ω) that increased with the number of thiophene spacer units; we hypothesize this trend is a direct result of the increased thiophene content resulting in decreased electron mobility and reduced number of reduction sites. Encouragingly, nitrogen adsorption experiments confirmed that the addition of thiophene spacers in the polymers resulted in a proportional increase in pore size, resulting in a concomitant decrease in diffusion resistance. Finally, TPA-1Th-NDI was used to fabricate preliminary symmetric supercapacitors. Galvanic cycling of these devices revealed a marginal capacitance, which reflects the oxidation kinetics at the positive electrode. EIS confirmed this resistance to oxidation; the R_{ct} and ESR values reached 420.3 Ω and 7.7 Ω, respectively.

Overall, this work represents a step forward in the use of synthetic chemistry to precisely control the structure and resultant device performance of polymeric supercapacitor electrodes. We have explored a technique to optimize the diffusivity resistance and redox kinetics in polymeric electrodes. With improvements in the material design, for instance through the design of electropolymerizable monomers that yield hyperbranched ambipolar polymers, efficient type III polymeric supercapacitors are feasible.

■ ASSOCIATED CONTENT

Supporting Information

^{1}H NMR information, GPC traces, cyclic voltammograms, and nitrogen adsorption/desorption plots for TPA-(n)Th-NDI polymers, galvanic cycling and stability, and Nyquist plots of symmetric supercapacitor fabricated from TPA-1Th-NDI polymer. The Supporting Information is available free of charge on the ACS Publications website at DOI: 10.1021/acs.macromol.5b01070.

■ AUTHOR INFORMATION

Corresponding Author

*E-mail luscombe@uw.edu (C.K.L.).

Funding

This material is based in part upon work supported by the State of Washington through the University of Washington Clean Energy Institute and the National Science Foundation (DMR-1407815 and CHE-1230615).

DOI: 10.1021/acs.macromol.5b01070
Macromolecules 2015, 48, 5196−5203

Notes

The authors declare no competing financial interest.

REFERENCES

(1) Chu, S.; Majumdar, A. *Nature* **2012**, *488* (7411), 294−303.
(2) Arico, A. S.; Bruce, P.; Scrosati, B.; Tarascon, J.-M.; van Schalkwijk, W. *Nat. Mater.* **2005**, *4* (5), 366−377.
(3) Wang, G.; Zhang, L.; Zhang, J. *Chem. Soc. Rev.* **2012**, *41* (2), 797−828.
(4) Nocera, D. G. *Chem. Soc. Rev.* **2009**, *38* (1), 13−15.
(5) Chen, H.; Cong, T. N.; Yang, W.; Tan, C.; Li, Y.; Ding, Y. *Prog. Nat. Sci.* **2009**, *19* (3), 291−312.
(6) Luo, B.; Wang, B.; Li, X.; Jia, Y.; Liang, M.; Zhi, L. *Adv. Mater.* **2012**, *24* (26), 3538−3543.
(7) Tarascon, J.-M.; Armand, M. *Nature* **2001**, *414* (6861), 359−367.
(8) Yamamoto, K.; Iriyama, Y.; Asaka, T.; Hirayama, T.; Fujita, H.; Fisher, C. A. J.; Nonaka, K.; Sugita, Y.; Ogumi, Z. *Angew. Chem., Int. Ed.* **2010**, *49* (26), 4414−4417.
(9) Nohma, T.; Kurokawa, H.; Uehara, M.; Takahashi, M.; Nishio, K.; Saito, T. *J. Power Sources* **1995**, *54* (2), 522−524.
(10) Abellan, P.; Mehdi, B. L.; Parent, L. R.; Gu, M.; Park, C.; Xu, W.; Zhang, Y.; Arslan, I.; Zhang, J.-G.; Wang, C.-M.; Evans, J. E.; Browning, N. D. *Nano Lett.* **2014**, *14* (3), 1293−1299.
(11) Lu, M.; Beguin, F.; Frackowiak, E. *Supercapacitors: Materials, Systems and Applications*; Wiley-VCH Verlag GmbH & Co. KGaA: Weinheim, 2013.
(12) Yan, J.; Wang, Q.; Wei, T.; Fan, Z. *Adv. Energy Mater.* **2014**, *4* (4), 1300816.
(13) Snook, G. A.; Kao, P.; Best, A. S. *J. Power Sources* **2011**, *196* (1), 1−12.
(14) Mastragostino, M.; Arbizzani, C.; Soavi, F. *J. Power Sources* **2001**, *97*−*98*, 812−815.
(15) Yu, Z.; Tetard, L.; Zhai, L.; Thomas, J. *Energy Environ. Sci.* **2015**, *8* (3), 702−730.
(16) Candelaria, S. L.; Shao, Y.; Zhou, W.; Li, X.; Xiao, J.; Zhang, J.-G.; Wang, Y.; Liu, J.; Li, J.; Cao, G. *Nano Energy* **2012**, *1* (2), 195−220.
(17) Davies, A.; Yu, A. *Can. J. Chem. Eng.* **2011**, *89* (6), 1342−1357.
(18) Sevilla, M.; Mokaya, R. *Energy Environ. Sci.* **2014**, *7* (4), 1250−1280.
(19) Yu, D.; Goh, K.; Wang, H.; Wei, L.; Jiang, W.; Zhang, Q.; Dai, L.; Chen, Y. *Nat. Nanotechnol.* **2014**, *9* (7), 555−562.
(20) Fisher, R. A.; Watt, M. R.; Ready, W. J. *ECS J. Solid State Sci. Technol.* **2013**, *2*, M3170−M3177.
(21) Zhang, D.; Miao, M.; Niu, H.; Wei, Z. *ACS Nano* **2014**, *8* (5), 4571−4579.
(22) Hao, P.; Zhao, Z.; Tian, J.; Li, H.; Sang, Y.; Yu, G.; Cai, H.; Liu, H.; Wong, C. P.; Umar, A. *Nanoscale* **2014**, *6* (20), 12120−12129.
(23) Lv, L.; Fan, Y.; Chen, Q.; Zhao, Y.; Hu, Y.; Zhang, Z.; Chen, N.; Qu, L. *Nanotechnology* **2014**, *25*, 235401.
(24) Huang, Y.; Liang, J.; Chen, Y. *Small* **2012**, *8* (12), 1805−1834.
(25) Hu, C.-C.; Liu, M.-J.; Chang, K.-H. *Electrochim. Acta* **2008**, *53* (6), 2679−2687.
(26) Park, B.-O.; Lokhande, C. D.; Park, H.-S.; Jung, K.-D.; Joo, O.-S. *J. Power Sources* **2004**, *134* (1), 148−152.
(27) Jang, J. H.; Kato, A.; Machida, K.; Naoi, K. *J. Electrochem. Soc.* **2006**, *153* (2), A321−A328.
(28) Patake, V. D.; Pawar, S. M.; Shinde, V. R.; Gujar, T. P.; Lokhande, C. D. *Curr. Appl. Phys.* **2010**, *10* (1), 99−103.
(29) Fang, W.-C.; Chen, K.-H.; Chen, L.-C. *Nanotechnology* **2007**, *18*, 485716.
(30) Wang, R.; Yan, X. *Sci. Rep.* **2014**, *4*, 3712.
(31) Chien, H.-C.; Cheng, W.-Y.; Wang, Y.-H.; Lu, S.-Y. *Adv. Funct. Mater.* **2012**, *22* (23), 5038−5043.
(32) Arbizzani, C. *J. Power Sources* **2001**, *100* (1−2), 164−170.
(33) Di Fabio, A.; Giorgi, A.; Mastragostino, M.; Soavi, F. *J. Electrochem. Soc.* **2001**, *148* (8), A845−A850.
(34) Balducci, A.; Henderson, W. A.; Mastragostino, M.; Passerini, S.; Simon, P.; Soavi, F. *Electrochim. Acta* **2005**, *50* (11), 2233−2237.
(35) Fusalba, F.; El Mehdi, N.; Breau, L.; Bélanger, D. *Chem. Mater.* **1999**, *11* (10), 2743−2753.
(36) Arbizzani, C.; Catellani, M.; Mastragostino, M.; Mingazzini, C. *Electrochim. Acta* **1995**, *40* (12), 1871−1876.
(37) Arbizzani, C.; Mastragostino, M.; Meneghello, L. *Electrochim. Acta* **1995**, *40* (13−14), 2223−2228.
(38) Talbi, H.; Just, P.-E.; Dao, L. H. *J. Appl. Electrochem.* **2003**, *33* (6), 465−473.
(39) Wang, J.; Xu, Y.; Chen, X.; Du, X. *J. Power Sources* **2007**, *163* (2), 1120−1125.
(40) Liu, T.; Finn, L.; Yu, M.; Wang, H.; Zhai, T.; Lu, X.; Tong, Y.; Li, Y. *Nano Lett.* **2014**, *14* (5), 2522−2527.
(41) Estrada, L. A.; Liu, D. Y.; Salazar, D. H.; Dyer, A. L.; Reynolds, J. R. *Macromolecules* **2012**, *45* (20), 8211−8220.
(42) DiCarmine, P. M.; Schon, T. B.; McCormick, T. M.; Klein, P. P.; Seferos, D. S. *J. Phys. Chem. C* **2014**, *118* (16), 8295−8307.
(43) Rudge, A.; Raistrick, I.; Gottesfeld, S.; Ferraris, J. P. *Electrochim. Acta* **1994**, *39* (2), 273−287.
(44) Stenger-Smith, J. D.; Lai, W. W.; Irvin, D. J.; Yandek, G. R.; Irvin, J. A. *J. Power Sources* **2012**, *220* (0), 236−242.
(45) Schon, T. B.; DiCarmine, P. M.; Seferos, D. S. *Adv. Energy Mater.* **2014**, *4* (7), 1301509.
(46) Chopin, S.; Chaignon, F.; Blart, E.; Odobel, F. *J. Mater. Chem.* **2007**, *17* (39), 4139−4146.
(47) Sahu, D.; Tsai, C.-H.; Wei, H.-Y.; Ho, K.-C.; Chang, F.-C.; Chu, C.-W. *J. Mater. Chem.* **2012**, *22* (16), 7945−7953.
(48) Shang, H.; Fan, H.; Liu, Y.; Hu, W.; Li, Y.; Zhan, X. *Adv. Mater.* **2011**, *23* (13), 1554−1557.
(49) Metri, N.; Sallenave, X.; Beouch, L.; Plesse, C.; Goubard, F.; Chevrot, C. *Tetrahedron Lett.* **2010**, *51* (50), 6673−6676.
(50) Wu, D.; Fu, R.; Zhang, S.; Dresselhaus, M. S.; Dresselhaus, G. *J. Non-Cryst. Solids* **2004**, *336* (1), 26−31.
(51) García, B. B.; Liu, D.; Sepehri, S.; Candelaria, S.; Beckham, D. M.; Savage, L. W.; Cao, G. *J. Non-Cryst. Solids* **2010**, *356* (33−34), 1620−1625.
(52) Roberts, M. E.; Wheeler, D. R.; McKenzie, B. B.; Bunker, B. C. *J. Mater. Chem.* **2009**, *19* (38), 6977−6979.
(53) Zhan, X.; Facchetti, A.; Barlow, S.; Marks, T. J.; Ratner, M. A.; Wasielewski, M. R.; Marder, S. R. *Adv. Mater.* **2011**, *23* (2), 268−284.
(54) Würthner, F.; Stolte, M. *Chem. Commun. (Cambridge, U. K.)* **2011**, *47* (18), 5109−5115.
(55) Suraru, S.-L.; Würthner, F. *Angew. Chem., Int. Ed.* **2014**, *53* (29), 7428−7448.
(56) Lin, C.-C.; Velusamy, M.; Chou, H.-H.; Lin, J. T.; Chou, P.-T. *Tetrahedron* **2010**, *66* (45), 8629−8634.
(57) Thalacker, C.; Röger, C.; Würthner, F. *J. Org. Chem.* **2006**, *71* (21), 8098−8105.
(58) Senkovskyy, V.; Tkachov, R.; Komber, H.; Sommer, M.; Heuken, M.; Voit, B.; Huck, W. T. S.; Kataev, V.; Petr, A.; Kiriy, A. *J. Am. Chem. Soc.* **2011**, *133* (49), 19966−19970.
(59) Hu, C.-C.; Chiang, H.-R.; Wang, C.-C. *J. Solid State Electrochem.* **2003**, *7* (8), 477−484.
(60) Hamelin, A.; Stoicoviciu, L.; Edens, G. J.; Gao, X.; Weaver, M. J. *J. Electroanal. Chem.* **1994**, *365* (1−2), 47−57.
(61) Kolb, D. M. *Angew. Chem., Int. Ed.* **2001**, *40* (7), 1162−1181.
(62) Weaver, M. J.; Gao, X. *Annu. Rev. Phys. Chem.* **1993**, *44* (1), 459−494.
(63) Aurbach, D. *J. Power Sources* **2000**, *89* (2), 206−218.
(64) Mastragostino, M.; Paraventi, R.; Zanelli, A. *J. Electrochem. Soc.* **2000**, *147* (9), 3167−3170.
(65) Laforgue, A.; Simon, P.; Fauvarque, J. F.; Sarrau, J. F.; Lailler, P. *J. Electrochem. Soc.* **2001**, *148* (10), A1130−A1134.
(66) Chen, S.; Zhitomirsky, I. *J. Power Sources* **2013**, *243* (0), 865−871.
(67) Redondo, M. I.; Breslin, C. B. *Corros. Sci.* **2007**, *49* (4), 1765−1776.
(68) Taberna, P. L.; Simon, P.; Fauvarque, J. F. *J. Electrochem. Soc.* **2003**, *150* (3), A292−A300.

DOI: 10.1021/acs.macromol.5b01070
Macromolecules 2015, 48, 5196−5203

(69) Ahmed, E.; Ren, G.; Kim, F. S.; Hollenbeck, E. C.; Jenekhe, S. A. *Chem. Mater.* **2011**, *23* (20), 4563−4577.
(70) Barrett, E. P.; Joyner, L. G.; Halenda, P. P. *J. Am. Chem. Soc.* **1951**, *73* (1), 373−380.

DOI: 10.1021/acs.macromol.5b01070
Macromolecules 2015, 48, 5196−5203